Macromolecules

ARTICLE

pubs.acs.org/Macromolecules

Viscoelastic Behavior of the Polymerized Ionic Liquid Poly(1-ethyl-3-vinylimidazolium bis(trifluoromethanesulfonylimide))

Kenji Nakamura,*[,†] Tatsuya Saiwaki,[†] Koji Fukao,[†] and Tadashi Inoue[‡]

[†]Department of Physical Sciences, Ritsumeikan University, Kusatsu, Shiga 525-8577, Japan

[‡]Department of Macromolecular Science, Graduate School of Science, Osaka University, Toyonaka, Osaka 560-0043, Japan

Supporting Information

ABSTRACT: Dynamic melt viscoelastic behavior for polymerized ionic liquids, poly(1-ethyl-3-vinylimidazolium bis(trifluoromethanesulfonylimide)) ($PC_2VITFSI$), with various molecular weights was investigated in the frequency/temperature range from the glass to the terminal region. Viscoelastic spectra at given temperatures for $PC_2VITFSI$ with lower molecular weight were able to be well superimposed on each other to make a master curve. $PC_2VITFSI$ with a molecular weight larger than 1.4×10^5 were entangled with each other, showing a rubbery region in the master curves. However, viscoelastic spectra for $PC_2VITFSI$ with higher molecular weight (larger than 2.2×10^5) were not superimposed in the rubbery and terminal regions due to the presence of two rubbery elastic origins, i.e., chain entanglement and ionic aggregates. The presence of huge ionic aggregates was unable to be confirmed by SAXS measurements, but the formation of ion pairs between a cation and an anion was supported by the WAXS profiles. Master curves of $PC_2VITFSI$ exhibited extended shoulders in the glass−rubber transition region; these arose from the relaxation mode due to segmental motions of positively charged polymer chains affected by neighboring $TFSI^-$ anions. The entanglement and critical molar mass of $PC_2VITFSI$ were determined to be 4.5×10^4 and 2.2×10^4, respectively.

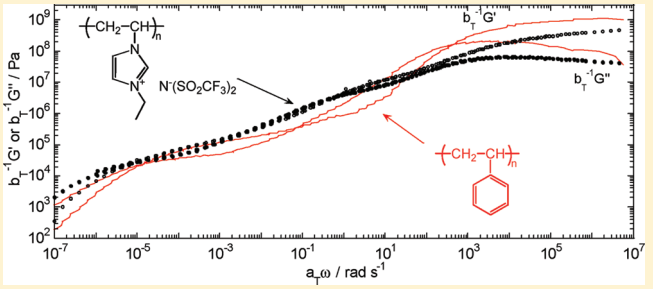

INTRODUCTION

Ionic liquids (IL) are organic molten salts formed by a pair of a soft cation and an anion.[1−4] Some ILs in the liquid state at room temperature display nonvolatility, nonflammability, and high electric conductivity. Many researchers have given significant attention to ILs and reported on their fundamental properties[5−7] and potential applications.[8−10]

Recently, polymerized ionic liquids (PILs) have also received research interest.[11] PILs can be chemically described as covalently bonded IL monomers. These systems are solid at room temperature and possess the characteristics of polymers. For example, PILs show lower conductivity rather than IL monomers due to their high viscosity.[11] On the other hand, PILs are easily downsized and molded by heating, similar to ordinary amorphous polymers. Ohno et al. have detailed the synthesis, characterization, and conductive behavior of many PIL species.[12] The application of PILs in devices such as capacitors,[13] electrochemical cells,[14] and macroporous films[15] has also been investigated. In addition, several reviews about PILs have recently been published.[16−20] However, despite this attention there have been relatively few reports regarding the physicochemical features of PILs.[21−23]

PILs can be classified as a polyelectrolyte species like sodium polystyrenesulfonate, in the sense that they consist of an electrolyte monomer unit. PILs with hydrophobic counterions, such as PF_6^-, are insoluble in water (unlike most polyelectrolytes) but soluble in some polar organic solvents.[24,25] These properties of PILs lead us to speculate that PILs can be regarded as model substances of solid-state polyelectrolytes, allowing us to study the bulk nature of the polyelectrolyte system; this is particularly important as the physiochemical properties of polyelectrolyte systems were previously limited to aqueous solutions because of their hygroscopicity and high glass transition temperature.[26]

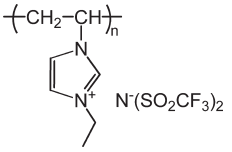

Figure 1. Chemical structure of poly(1-ethyl-3-vinylimidazolium bis(trifluoromethanesulfonylimide)) ($PC_2VITFSI$).

We have focused on the kinetic properties of PILs; we have previously reported on the dielectric relaxation (DR) behavior of poly(1-ethyl-3-vinylimidazolium bis(trifluoromethane sulfonylimide)) ($PC_2VITFSI$) (Figure 1) to elucidate their microdynamics.[27] $PC_2VITFSI$ showed two DR modes; the fast and slow DR modes were attributed to the rotational motion of the polymer side

Received: July 14, 2011
Revised: August 24, 2011
Published: September 08, 2011

chain and the segmental motion of the polymer, respectively. Both conductivity and the relaxation time of the slow mode showed Arrhenius temperature dependence and had a similar activation energy. This indicates that ion conduction correlates to the origin of the slow DR mode.

In this study, we investigate the viscoelastic behavior[28,29] of PC_2VITFSI over a wide range of frequencies (temperatures) from the glass to the terminal region to clarify the macrodynamics of the PIL melt, i.e., the bulk polyelectrolyte system. Since the rheological behavior of ordinary amorphous polymers is strongly dependent on the molecular weight of the polymers,[30] we prepared PC_2VITFSI with various molecular weights. While there are some reports regarding the viscoelastic behavior of polymer/IL solutions,[31,32] PIL systems have not been investigated. The only pertinent paper on PIL rheology investigated the temperature-dependent viscoelastic behavior of a triblock copolymer with a PIL midblock.[33] The viscoelastic behavior of PC_2VITFSI was compared with those observed in polystyrene and in ionomers[34] that include a few electrolyte monomer units in the polymer chain and are classified as polyelectrolytes. Ionomers have been known to form ion aggregates consisting of a charged monomer unit and a counterion in the melt to show a specific scattering peak against the X-ray measurement.[34] Their viscoelastic behavior is strongly affected by the presence of aggregates. Hence, we performed small- and wide-angle X-ray scattering (SAXS and WAXS) measurements to obtain the structural information and elucidate its essential viscoelastic aspects. We also compare the viscoelastic spectra with the DR spectra[27] to discuss their entire dynamics. This comparison allowed us to reconsider the previous attribution of the slow DR mode and accept that the origin of the slow DR mode is not the segmental motion of polymers, but lifetime of ion pairs formed between a cation monomer unit and a counteranion.

EXPERIMENTAL SECTION

Materials. 1-Vinylimidazole was purchased from Tokyo Kasei (Tokyo). Bromoethane and 2,2′-azobis(isobutyronitrile) (AIBN) were purchased from Wako Pure Chemicals (Osaka). Lithium bis(trifluoromethanesulfonyl)imide (LiTFSI) was purchased from Kanto Chemical (Tokyo). DMSO-d_6 and acetone-d_6 were purchased from ISOTEC Inc. (Cambridge) and used as a solvent for NMR measurements. Polydispersed polystyrene (PS) with the number-average molecular weight M_n of 2.4×10^5 and PDI = 1.5 was kindly supplied by Mitsuitoatsu Chemical. All of the reagents were used without further purification.

Synthesis. 1-Ethyl-3-vinylimidazolium bromide was prepared by refluxing the mixture of 1-vinylimidazole (11.6 g, 123 mmol) and excess bromoethane (27.0 g, 247 mmol) in a methanol solution (8 mL) at 50 °C for 2 days.[11] After the methanol and unreacted bromoethane were completely evaporated from the solution, 1-ethyl-3-vinylimidazolium bromide was dried under vacuum at 70 °C (99% yield). 1-Ethyl-3-vinylimidazolium bromide (24.8 g, 122 mmol) was dissolved in an aqueous solution (60 mL) with a slight excess of LiTFSI (44.2 g, 154 mmol) and stirred for 4 days at room temperature. The resultant ionic liquid phase of 1-ethyl-3-vinylimidazolium bis(trifluoromethanesulfonyl)imide (C_2VITFSI) was separated from the aqueous phase and washed with water five times. After completely evaporating the remaining water, C_2VITFSI was dried under vacuum at 50 °C (82% yield). The purity of C_2VITFSI was confirmed using ^{1}H NMR measurements[24,27] in DMSO-d_6 (Figure S1 in the Supporting Information) and elemental analysis measurements. Found (%): C, 27.41; H, 2.53; N, 10.49; calcd for $C_9H_{11}N_3O_4S_2F_6$: C, 26.80; H, 2.75; N, 10.42. The absence of AgBr precipitation after the addition of an aqueous $AgNO_3$ solution indicated that bromide salts were eliminated from the C_2VITFSI.

Table 1. Molar Ratio of the Monomer to the Initiator M/I, Volume Ratio of the Monomer to the Solvent M/S, Polymerization Solvent, Intrinsic Viscosity $[\eta]$,[a] Viscosity-Average Molecular Weight M_v,[b] and the Glass Transition Temperature T_g for the Polymerized PC_2VITFSI

M/I	M/S	solvent	$[\eta]$/cm^3 g^{-1}	$M_v/10^3$	T_g/°C
200	0.19	DMF	2.92	2.4	33
25	1.37	MEK	10.55	19	51
50	2.07	MEK	17.60	45	56
50	3.38	MEK	23.35	71	56
50	3.65	MEK	35.01	140	55
25	3.00	DMSO	47.21	220	56
100	3.21	DMSO	63.55	360	56
200	9.76	DMSO	76.18	480	56

[a] In MEK solution containing 75 mM LiTFSI. [b] Employing $[\eta] = KM_v^a$ with parameters of $K = 2.3 \times 10^{-2}$ cm^3 g^{-1} and $a = 0.62$.[35]

PC_2VITFSI was synthesized via the free radical polymerization of C_2VITFSI. Polymerizations were initiated by AIBN in DMSO, DMF, or a methyl ethyl ketone (MEK) solution at 60 °C for 16 h. Solvent species and the molar ratio of the monomer to the initiator (M/I) and the volume ratio of the monomer to the solvent (M/S) were varied to obtain polymers with various molecular weight, as summarized in Table 1. PC_2VITFSI was precipitated by pouring the resultant solution into an excess ethanol solution. Repeating the precipitation from acetone to ethanol solution purified the crude PC_2VITFSI. The product purity was confirmed using ^{1}H NMR measurements in acetone-d_6 (Figure S1 in the Supporting Information).[24,27]

Measurements. The intrinsic viscosity ($[\eta]$) of PC_2VITFSI was measured using an Ubbelohde dilution viscometer at 30 °C in MEK containing 75 mM LiTFSI. The value of the viscosity-average molecular weight (M_v) for PC_2VITFSI was estimated by employing the Mark–Houwink–Sakurada equation $[\eta] = KM_v^a$ with parameters of $K = 2.3 \times 10^{-2}$ cm^3 g^{-1} and $a = 0.62$. These parameters were determined in a polystyrene/MEK solution at 30 °C.[35] Table 1 includes $[\eta]$ and M_v values for polymerized PC_2VITFSI. It is important to note that the polydispersity of the PC_2VITFSI series is unclear and certainly broad, as is its characteristic of radical polymerization.

^{1}H NMR measurements were performed using an NMR spectrometer (JNM-ECA-400, JEOL, Tokyo, Japan) with a proton resonance frequency of 400 MHz to characterize the synthesized ILs and PILs at 30 °C.

The glass transition temperature (T_g) of PC_2VITFSI was estimated using a differential scanning calorimeter (DSC) (EXSTAR DSC6000, SII, Chiba, Japan) at a heating and cooling rate of 10 K/min. The measurement temperature ranged from −20 to 120 °C. Resultant DSC profiles were similar to that found using $M_v = 4.2 \times 10^4$ in our previous study.[27] The T_g values of the PC_2VITFSI series were determined from the midpoint of the total heat flow curve in the thermal transition region and are tabulated in Table 1. T_g values increase with increasing M_v and become to be constant value 56 °C above $M_v = 4.5 \times 10^4$ as is the case with the ordinary amorphous polymers predicted by Flory–Fox theory.

SAXS and WAXS measurements were performed on the BL40B2 beamline at SPring-8. A wavelength of X-ray was 0.9 Å for both SAXS and WAXS measurements. The detector used in our measurements was a combination of an X-ray image intensifier and a CCD camera. The spatial resolution of the CCD camera was 0.106 mm in both the horizontal and vertical directions. The camera lengths were 2231 and 107 mm for the SAXS and WAXS measurements, respectively. The obtained scattering data were corrected in order to remove variations in intensities of incident X-rays and the contribution of background scattering.

Density (d_{PIL}) of $PC_2VITFSI$ was determined using pycnometer with a water solvent at 25 °C.

Dynamic viscoelastic measurements were performed using strain-controlled rheometers (ARES, TA Instruments, New Castle, DE) and (Rheosol-G2000, UBM, Kyoto, Japan) equipped with a parallel plate geometry with a diameter of 4 and 10 mm under a nitrogen atmosphere for temperature ranged from 50 to 300 °C. The angular frequency (ω) was varied from 6.28×10^{-1} to 6.28×10^{2} rad s^{-1} for the ARES and 6.28×10^{-2} to 6.28×10^{1} rad s^{-1} for the Rheosol-G2000. The storage and loss moduli (G' and G''), which obeyed a linear viscoelastic response, were used for analysis. Instrument compliance is known to be an important issue in the rheological measurements in the glassy zone. Following the method reported by McKenna et al.,[36−38] we corrected the instrument compliance.

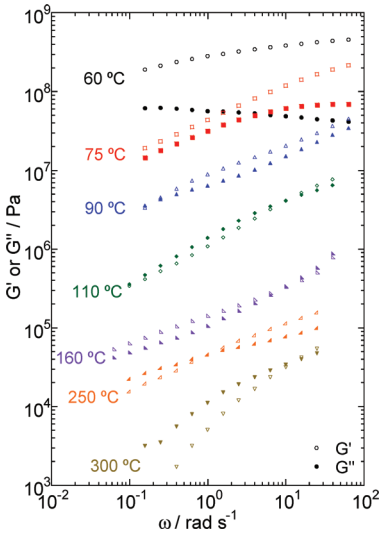

Figure 2. Dependence of the storage and loss moduli G' and G'' on angular frequency ω for $PC_2VITFSI$ with $M_v = 1.4 \times 10^5$ at various temperatures.

The samples for density, rheology, and X-ray measurements were prepared as follows: the $PC_2VITFSI$/acetone solution was cast onto a Teflon Petri dish. After slow evaporation of the solvent, the plane films were dried under vacuum at 80 °C for at least 1 day. They were then molded using a hot press at T_g + 45 °C, with or without a 1.5 mm SUS spacer to make a plane film for density and rheology or X-ray measurements, respectively. The resulting $PC_2VITFSI$ films were transparent with a slight yellow tinge.

RESULTS

Viscoelastic Behavior. Figure 2 shows the dependence of G' and G'' on ω for $PC_2VITFSI$ with $M_v = 1.4 \times 10^5$ at various temperatures. These data are superimposed to make master curves of $b_T^{-1}G'$ and $b_T^{-1}G''$ against $a_T\omega$ using time and modulus scale multiplicative shift factors, a_T and b_T. Figure 3 shows the master curves for $PC_2VITFSI$ with $M_v = 1.4 \times 10^5$ at the reference temperature, T_0, of 90 °C (= T_g + 35 °C). Figure 3 includes master curves for polydispersed polystyrene (PS) with the number-average molecular weight $M_n = 2.4 \times 10^5$ at a T_0 of 130 °C as well as the tan δ (= G''/G') curves.

The master curves for $PC_2VITFSI$ seem to succeed in the superposition excluding the data at 300 °C. The temperature dependence of a_T is well reproduced by the WLF equation.[39] The presence of a rubbery region for $PC_2VITFSI$ with $M_v = 1.4 \times 10^5$ in the frequency range of $10^{-5} < a_T\omega < 10^{-3}$ rad s^{-1} indicates that the $PC_2VITFSI$ polymer chains are fully entangled with each other. In contrast to the finding that the tan δ curve for PS shows a peak at $a_T\omega = 10$ rad s^{-1}, $PC_2VITFSI$ shows two peaks at $a_T\omega$ = 200 and 0.1 rad s^{-1}. Moreover the glass−rubber transition region for $PC_2VITFSI$ is broader than that for PS. These indicate that $PC_2VITFSI$ reveals an unusual relaxation, which is not observed in ordinary amorphous polymers, in the glass−rubber transition region.

The glassy modulus of the $PC_2VITFSI$ with $M_v = 1.4 \times 10^5$ is estimated to be 0.5 GPa. This value is smaller than those for PS

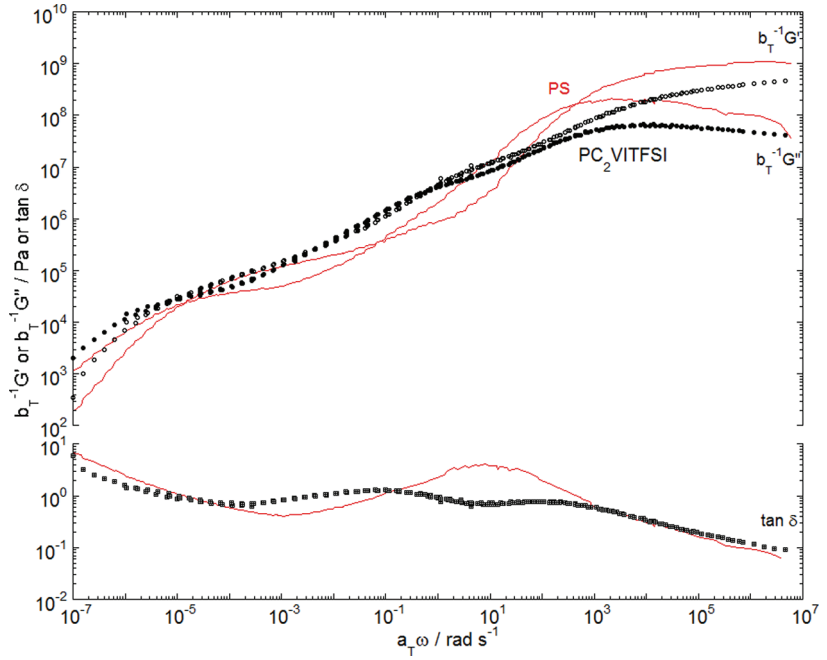

Figure 3. Master curves of $b_T^{-1}G'$, $b_T^{-1}G''$, and tan δ for $PC_2VITFSI$ with $M_v = 1.4 \times 10^5$ at the reference temperature T_0 = 90 °C. Red solid lines indicate the master curves for polystyrene (PS) with $M_n = 2.4 \times 10^5$ at T_0 = 130 °C.

dx.doi.org/10.1021/ma201611q |Macromolecules 2011, 44, 7719–7726

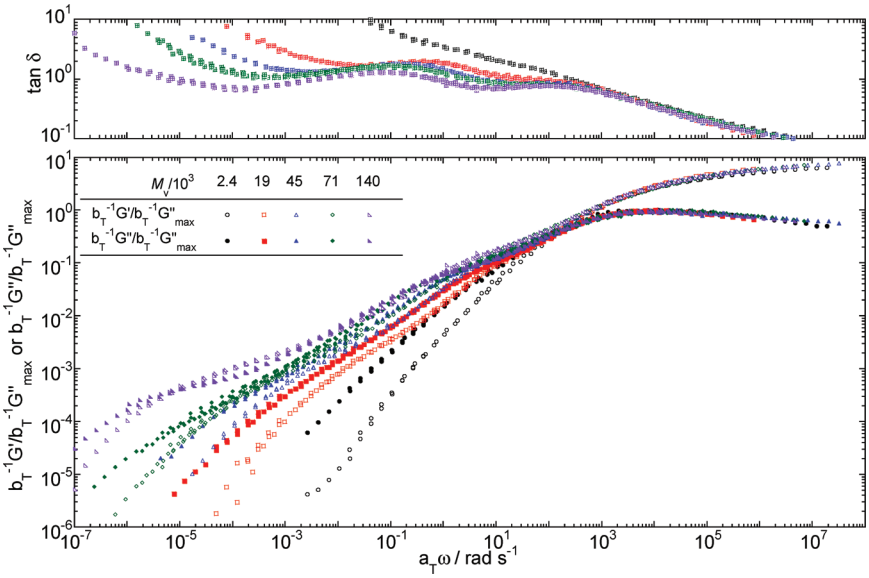

Figure 4. Normalized master curves of $b_T^{-1}G'/b_T^{-1}G''_{max}$ and $b_T^{-1}G''/b_T^{-1}G''_{max}$ and tan δ master curves for $PC_2VITFSI$ with various molecular weights at T_0 of T_g + 35 °C.

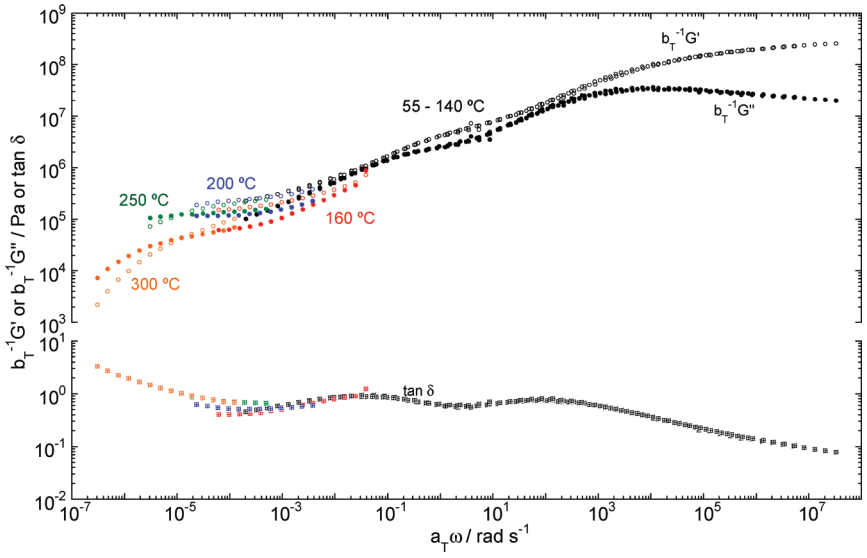

Figure 5. Pseudo master curves of $b_T^{-1}G'$, $b_T^{-1}G''$, and tan δ for $PC_2VITFSI$ with $M_v = 3.6 \times 10^5$ at T_0 of T_g + 35 °C.

(ca. 1 GPa) and other amorphous polymers.[40] Since values of the glassy modulus for $PC_2VITFSI$ series ranged from 0.3 to 0.7 GPa and were slightly dependent on M_v, the master curves were normalized using the maximum value of the G'' curve, G''_{max}, when the M_v-dependent viscoelastic behavior is considered. Figure 4 shows the normalized master curves $b_T^{-1}G'/b_T^{-1}G''_{max}$ and $b_T^{-1}G''/b_T^{-1}G''_{max}$ as well as tan δ curves on $a_T\omega$ for $PC_2VITFSI$ with various M_v values ($\leq 1.4 \times 10^5$) at T_0 of T_g + 35 °C. One confirms that the time−temperature superposition principle holds for a $PC_2VITFSI$ series with $M_v \leq 1.4 \times 10^5$. The normalized master curves for $PC_2VITFSI$ with $M_v = 2.4 \times 10^3$ seem to have only a glass and terminal region, similar to low-molecular-weight molecular glass. The additional shoulders in the master curves due to the glass−rubber transition region appear for the $PC_2VITFSI$ with $M_v = 1.9 \times 10^4$ and are extended to the lower frequency region with increasing M_v. The tan δ curves for $PC_2VITFSI$ with M_v values larger than 1.9×10^4 show double peaks.

Shapes of normalized master curves for $PC_2VITFSI$ with $M_v \geq 4.5 \times 10^4$ correspond with each other in the frequency range of $10 < a_T\omega < 10^3$ rad s^{-1}. This indicates that the short-scale segmental dynamics of enough long polymer chains are independent of M_v values even if polymer chains are charged and surrounded by ions. Since the glass transition behavior essentially lies in the segmental dynamics, it is reasonable that T_g values above $M_v = 4.5 \times 10^4$ are saturated (Table 1).

The $b_T^{-1}G'/b_T^{-1}G''_{max}$ curves for $PC_2VITFSI$ with M_v smaller than 7.1×10^4 seem to lack the rubbery region. This finding leads ones to speculate that their polymer chains are unable to be entangled with each other. However, as concluded in the Discussion part, the entanglement and critical molar mass of $PC_2VITFSI$ is lower than 7.1×10^4.

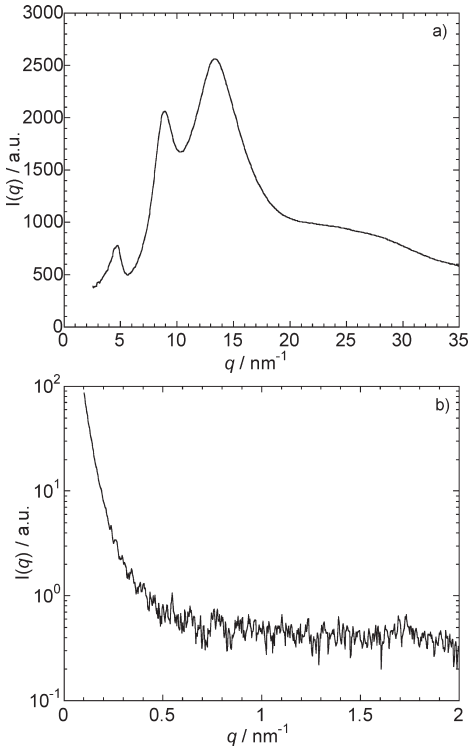

Figure 6. (a) WAXS and (b) SAXS diffraction spectra for $PC_2VITFSI$ with $M_v = 3.6 \times 10^5$ at 25 °C.

The time−temperature superposition principle failed for the $PC_2VITFSI$ with high M_v. Figure 5 shows pseudo master curves of $b_T^{-1}G'$, $b_T^{-1}G''$, and tan δ for $PC_2VITFSI$ with $M_v = 3.6 \times 10^5$ at T_0 of T_g + 35 °C as a typical example. Viscoelastic spectra at temperatures ranging from 55 to 140 °C, which corresponds to the glassy and glass−rubber transition region, were well superimposed; this was in contrast with those at temperatures above 160 °C, corresponding to the rubbery region. At high temperatures, the magnitudes of $b_T^{-1}G'$ and $b_T^{-1}G''$ were strongly dependent on applied strain and tended to decrease with increasing strain. These results indicate that $PC_2VITFSI$ system possesses another elasticity origin in addition to that due to the chain entanglement. The same failure of the superposition in the rubbery region was observed for $PC_2VITFSI$ with $M_v \geq 2.2 \times 10^5$.

Small- and Wide-Angle X-ray Scattering Measurements. Figure 6a,b shows WAXS and SAXS diffraction spectra for $PC_2VITFSI$ with $M_v = 3.6 \times 10^5$ at 25 °C. No peaks are observed in the SAXS profile. In contrast, the WAXS profile shows three peaks at scattering vectors, q, of 4.76, 8.91, and 13.42 nm^{-1} and shoulders at $q \geq 20$ nm^{-1}. The Bragg spacing of the three WAXS peaks is estimated to be 1.33, 0.70, and 0.47 nm, respectively.

Elabd and co-workers have also performed X-ray scattering measurements of PILs with varying counterion species and charge density of a polymer chain.[23] Two scattering peaks were observed around q = 4.5 and 14.0 nm^{-1} for their PILs irrespective of counterion species and charge density of a chain; accordingly, they attributed the former peak to the local ordering of alkyl segments and the latter one to the amorphous halo. Since the q values of the two peaks observed in their PILs are similar to those observed in our $PC_2VITFSI$, the lowest and highest q peaks observed in $PC_2VITFSI$ would reflect the local ordering of chains and amorphous halo, respectively.

Although Elabd only mentioned the two peaks above, their WAXS profiles seemed to yield a new peak between the two peaks with increasing $TFSI^-$ content in their PIL copolymers bearing both $TFSI^-$ and BF_4^- counteranions.[23] The q value of the new peak (ca. 9.0 nm^{-1}) for their PILs are close to that of the intermediate peak for $PC_2VITFSI$ (8.91 nm^{-1}); consequently, the intermediate peak for $PC_2VITFSI$ should relate to the $TFSI^-$ anion. This assumption is supported by Gibson's study, which reported that imidazolium polyesters with $TFSI^-$ also exhibited three WAXS peaks with similar q values.[41]

In order to clarify the origin of the intermediate WAXS peak, we evaluate the cation and anion size of $PC_2VITFSI$ as follows. The volume of the $PC_2VITFSI$ monomer unit v_m is calculated to be 0.43 nm^3 from the density of bulk $PC_2VITFSI$ d_{PIL}, 1.55 g cm^{-3}, using the relationship $v_m = M_m/d_{PIL}N_a$, where M_m and N_a are the molecular weight of the $PC_2VITFSI$ monomer unit and Avogadro's number. Then, the volume of the 1-ethyl-3-vinylimidazolium cation (C_2VI^+) is determined to be 0.20 nm^3 using the previously determined $TFSI^-$ volume, 0.23 nm^3.[42] The evaluated van der Waals radii of the C_2VI^+ and $TFSI^-$ ion, assuming a spherical shape, are 0.36 and 0.38 nm, respectively. The interionic distance between C_2VI^+ and $TFSI^-$, 0.74 nm, is close to the Bragg spacing of the intermediate WAXS peak (0.70 nm). This suggests that the intermediate peak reflects the ion-pair distance formed between C_2VI^+ and $TFSI^-$.

DISCUSSION

Comparison with the Ionomer System. It has been reported that ionomers form ion aggregates consisting of their ionic groups due to the electrostatic attraction caused between them.[34,43,44] The SAXS profile of the ionomer system typically possessing small metal counterions shows a scattering peak, denoted as an ionic peak, reflecting the spatial distance between ionic aggregates.[45,46] In contrast, ionomers with large counterions did not show any clear ionic peaks because larger counterions form fewer (or weaker) aggregates.[47] Since $PC_2VITFSI$ has a soft and large counteranion ($TFSI^-$) and exhibits no SAXS peak (Figure 6b), one supposes that $PC_2VITFSI$ forms only a few ion aggregates, if any at all. PILs consist of only electrolyte monomer units (in contrast to ionomers, which are comprised of a few, mainly neutral, electrolyte monomers); as a result, the spatial correlation regarding the aggregates in $PC_2VITFSI$ was too short to exhibit the SAXS ionic peak, but the WAXS ionic peak corresponding to the ion-pair distance was apparent (Figure 6a). X-ray studies provided implicit proof of the existence of ion aggregates, which was confirmed and is discussed below.

Ion aggregations in an ionomer system strongly affect its viscoelastic behavior.[48−50] Taking the ionomer system of partially sulfonated polystyrenes with sodium anion (P(St/SSNa)) as an example, the magnitude of the plateau modulus and terminal relaxation time for P(St/SSNa) are higher than those for PS and increase with increasing degree of sulfonation.[51] This behavior is interpreted as the presence of two elastic mechanisms, i.e., entanglement of polymer chains and physically cross-linked ion aggregates— the ionic modulus.[49] If the temperature dependence of the lifetime of ion aggregates differs from that of polymer reptation time, as is often the case, the resultant (pseudo) master curve clearly shows two relaxation modes[48,49,52,53] and seems to fail in superposition.[48,50,51] According to Colby's study, ionomers with larger counterions showed good superposition but displayed shorter time scales for the terminal response due to

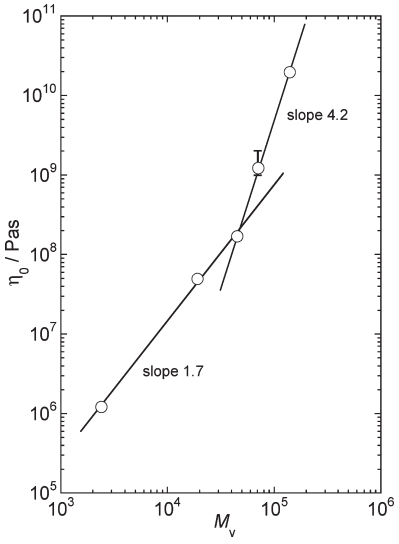

Figure 7. Relationship between η_0 and M_v for $PC_2VITFSI$ at a temperature of T_g + 35 °C.

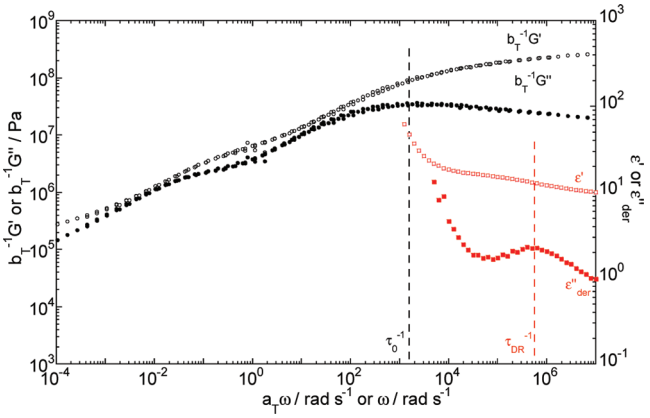

Figure 8. Dependence of the viscoelastic master curves, $b_T^{-1}G'$ and $b_T^{-1}G''$, on $a_T\omega$ and the dielectric spectra, ε' and ε''_{der}, on ω for $PC_2VITFSI$ with $M_v = 3.6 \times 10^5$ at 80 °C.

fewer ion-pair formations in comparison with ionomers with smaller and metal counterions.[47] Weiss and co-workers also reported that the use of the smaller counterion X^- for the P(St/SSX) oligomer enhanced ion association, yielding a longer terminal relaxation time even if the polymer chains were too short to fully entangle with each other.[54]

The above rheological features of ionomers give us some insight into the viscoelastic behavior of $PC_2VITFSI$. The good superposition of viscoelastic spectra for $PC_2VITFSI$ with $M_v \leq 1.4 \times 10^5$ lies in the use of the soft and large counteranion $TFSI^-$ (Figure 4). On the other hand, the failure of the superposition in the rubbery region observed in $PC_2VITFSI$ with $M_v \geq 2.2 \times 10^5$ at high temperatures indicates the presence of ionic aggregates, which dissociate with increasing temperature and applied strain (Figure 5). This assumption is supported by the result that the magnitude of the rubbery modulus for $PC_2VITFSI$ with $M_v = 3.6 \times 10^5$ is higher than that with $M_v = 1.4 \times 10^5$, indicating the ionic modulus enhances the rubbery modulus.

In terms of the ionomer's rheological properties,[49,52,53] the relaxation mode observed in the glass−rubber transition region in $PC_2VITFSI$ seems to be the ionic modulus. Although we believe that this relaxation mode correlates to ionic interactions, the above explanation does have shortcomings: the relaxation mode in the transition region was observed in all $PC_2VITFSI$ systems with $M_v \geq 1.9 \times 10^4$, while the ionic modulus effect enhancing the rubbery modulus was observed only in the $PC_2VITFSI$ with $M_v \geq 2.2 \times 10^5$. Moreover, good superposition of the viscoelastic spectra was found in the $a_T\omega$ range, corresponding to the glass and transition region, irrespective of the M_v values of $PC_2VITFSI$, whereas failure of superposition was confirmed in the rubbery region for $PC_2VITFSI$ with $M_v \geq 2.2 \times 10^5$ due to the presence of the ionic modulus. These findings indicate that the origin of the relaxation mode in the transition region differs from the ionic modulus.

Thus, we propose that the viscoelastic behavior of $PC_2VITFSI$ consists of two different ionic contributions. The first contribution is the classical ionic modulus due to the ionic aggregations, whose cross-links enhance the rubbery modulus. The second contribution is the relaxation mode in the transition region, reflecting the short-scale dynamics of the segmental motion of a charged chain affected by neighboring $TFSI^-$ because the average distances between neighboring C_2VI^+ units or between a C_2VI^+ and a $TFSI^-$ (ca. 0.70 nm) are shorter than the Kuhn length of a polymer (1−2 nm for ordinary polymers).[40] This assumption is supported by the success of the superposition of viscoelastic spectra in the glass and transition region; i.e., a_T values for the transition relaxation mode have the same temperature dependence as that for the segmental motion of a polymer chain.

Critical and Entanglement Molar Mass of $PC_2VITFSI$. It has been known that the shape of the viscoelastic spectra strongly depends on the molecular weight distribution, especially in the terminal and rubbery regions.[55] On the other hand, the values of zero-shear viscosity η_0 obtained by the following relationship are dependent only on the molecular weight and are independent of the molecular weight distribution:

$$\eta_0 = \lim_{\omega \to 0} \frac{G''}{\omega} \tag{1}$$

Figure 7 shows the relationship between η_0 and M_v for $PC_2VITFSI$ at T_0 of T_g + 35 °C. Since nonlinear viscoelastic behavior in the terminal and rubbery region hindered the evaluation of precise η_0, we estimated η_0 values for the $PC_2VITFSI$ with $M_v \leq 1.4 \times 10^5$. Figure 7 shows relationships $\eta_0 \propto M_v^{1.6}$ in the range of $M_v \leq 4.5 \times 10^4$ and $\eta_0 \propto M_v^{4.0}$ in the range of $M_v \geq 4.5 \times 10^4$; this suggests that the critical molar mass M_c for $PC_2VITFSI$ is 4.5×10^4. The slopes of η_0 for $PC_2VITFSI$ are higher than those for linear polymer melts, i.e., $\eta_0 \propto M^{1.0}$ ($M \leq M_c$) and $\eta_0 \propto M^{3.4}$ ($M \geq M_c$),[29,40] indicating that the origins of the viscosity for $PC_2VITFSI$ are not only friction and entanglement of polymer chains but also electrostatic interactions between charged polymer chains and counterions.

The entanglement molar mass M_e for $PC_2VITFSI$ can be evaluated using the following relationship[29,40]

$$M_e = \frac{\rho RT}{G_N} \tag{2}$$

where ρ is the density (concentration) of the polymer, R is the gas constant, T is the absolute temperature, and G_N is the magnitude of the plateau modulus. G_N values for ordinary amorphous polymers with enough high molecular weight are independent of the molecular weight because G_N values reflect

the entanglement density of polymer chains. However, the rubbery modulus for $PC_2VITFSI$ depends on M_v values due to the presence of ionic aggregates. Here, we roughly estimate the G_N value for the $PC_2VITFSI$ at 0.1 MPa from the master curves of $PC_2VITFSI$ with $M_v = 1.4 \times 10^5$ (Figure 3), which would not include the contribution of the ionic modulus because they show the clear rubbery region keeping well superposition principle. This G_N value is half of that for PS (0.2 MPa),[40] which suggests the validity of the G_N value for $PC_2VITFSI$ because the density of PC_2VI^+ polymer chain (0.72 g cm^{-3}) is approximately half of the bulk $PC_2VITFSI$ d_{PIL} (1.55 g cm^{-3}). The M_e value of the $PC_2VITFSI$ at 90 °C is calculated to be 2.2×10^4 using eq 2. We can confirm that the relationship $M_c/M_e \cong 2$ also holds for $PC_2VITFSI$ as is the case for ordinary amorphous polymers.[29,40] This finding implies the validity of M_c and M_e values.

One supposes that the absence of the rubbery region in the master curves for $PC_2VITFSI$ with $M_v = 7.1 \times 10^4$ (Figure 4) contradicts the finding of $M_c = 4.5 \times 10^4$ (Figure 7) because ordinary polymer chains with the molecular weight above M_c entangle with each other.[29,40] In contrast to low-disperse polymers, polydisperse polymers show unclear rubbery region due to the presence of low-molecular-weight polymer components even if their molecular weight is somewhat higher than M_c.[55] Since the $PC_2VITFSI$ samples are polydisperse polymers, it is natural that the master curves for $PC_2VITFSI$ with $M_v = 7.1 \times 10^4$ seems to lack a rubbery region.

Comparison between Viscoelastic and Dielectric Behavior. In order to associate the macrodynamics with the microdynamics of PILs, we compare the viscoelastic spectra with the DR spectra obtained in our previous study[27] for $PC_2VITFSI$. Figure 8 includes both viscoelastic master curves and DR spectra for $PC_2VITFSI$ with $M_v = 3.6 \times 10^5$ at 80 °C. The DR spectra consist of the real and the conduction-free imaginary parts of the complex dielectric permittivity, ε' and ε''_{der}, calculated using the relationship $\varepsilon''_{der} = -0.5\pi\, d(\varepsilon'(\omega))/d(\ln \omega)$.[56] According to our previous study,[27] the slow DR mode observed around $\omega = 5.0 \times 10^5$ rad s^{-1} in Figure 8 reflected the segmental motion of polymer chains.

Rouse theory predicts that the segmental relaxation time obtained from the DR measurement is 2 times longer than that estimated by the rheological measurement.[29,57] The relaxation time of the Kuhn monomer τ_0, which corresponds to the reciprocal of the maximum peak frequency in a G'' curve around the glass region, means the shortest stress relaxation time in the Rouse model, i.e., the segmental relaxation time in terms of rheology.[40,58] The estimated τ_0 value, 0.77 ms, is about 2600 times longer than the relaxation time of the slow DR mode, τ_{DR}, of 2 μs for $PC_2VITFSI$ at 80 °C (Figure 8). This indicates that the DR mode does not originate from the segmental motion of $PC_2VITFSI$ polymers, suggesting that our original assessment was incorrect.

The finding that both the slow DR time and the conductivity showed the Arrhenius temperature dependence with similar activation energy suggests that the slow DR mode should cooperate with the conductive behavior. The slow DR mode is therefore attributed to the motion of the ion pair formed between a positively charged monomer unit and a counteranion. The repetition of the ion-pair formation and dissociation process supports the transportation of the $TFSI^-$ anion.[27] This is consistent with the previous DR result that dielectric strength due to the slow DR mode increases with increasing temperature because quadrupoles can be expected to form through dipole–dipole interactions of neighboring ion pairs at low temperatures and dissociate into two ion pairs with increasing temperature.[59] The strong effect of the conductivity and electrode polarization behavior should mask the DR mode due to the segmental motion of $PC_2VITFSI$ chains in the DR spectra. The segmental DR mode should show Vogel–Fulcher–Tammann type temperature dependence as is the case for the temperature dependence of a_T in the viscoelastic spectra.

CONCLUSION

We investigated the dynamic viscoelastic behavior of the polymerized ionic liquid poly(1-ethyl-3-vinylimidazolium bis(trifluoromethanesulfonylimide)) ($PC_2VITFSI$) with various viscosity average molecular weights, M_v, over frequencies/temperatures ranging from the glass to the fluid state. The time–temperature superposition principle held for $PC_2VITFSI$ with lower $M_v \leq 1.4 \times 10^5$ but failed for those with $M_v \geq 2.2 \times 10^5$. The failure of the superposition can be explained by the origination of the rubbery elastic behavior in the presence of ionic aggregates in addition to polymer entanglement. SAXS and WAXS studies suggested the absence of huge ionic aggregates but showed the presence of ion-pair formation with an ionic distance of ~0.70 nm. Since this distance is shorter than the segmental length, we concluded that the segmental motion of positively charged polymer chains were affected by neighboring $TFSI^-$ anions and exhibited the shoulder in glass–rubber transition region on the viscoelastic master curve. Critical and entanglement molar mass, M_c and M_e, for $PC_2VITFSI$ were determined to be 4.5×10^4 and 2.2×10^4, respectively; the relationship $M_c/M_e \cong 2$ holds as is the case for ordinary amorphous polymers. The comparison between the viscoelastic master curves and dielectric relaxation spectra showed that the slow dielectric relaxation mode was not derived from the segmental motion of the $PC_2VITFSI$ chains—as was previously thought—but also from the lifetime of ion pairs.

ASSOCIATED CONTENT

Supporting Information. Figure S1 with the ^1H NMR spectra for synthesized $C_2VITFSI$ and $PC_2VITFSI$. This material is available free of charge via the Internet at http://pubs.acs.org.

AUTHOR INFORMATION

Corresponding Author
*E-mail: kenjin@se.ritsumei.ac.jp.

ACKNOWLEDGMENT

This work was supported by a Grant-in-Aid for Young Scientists (B) (No. 21750131) from the Japan Society for the promotion of Science. The synchrotron radiation experiments were performed at the SPring-8 with the approval of the Japan Synchrotron Radiation Research Institute (JASRI).

REFERENCES

(1) Wilkes, J. S.; Zaworotko, M. *J. Chem. Soc., Chem. Commun.* **1992**, 965.
(2) Welton, T. *Chem. Rev.* **1999**, *99*, 2071.
(3) Wasserscheid, P.; Welton, T. *Ionic Liquids in Synthesis*; Wiley-VCH: Weinheim, 2003.
(4) Ohno, H., Ed. *Electrochemical Aspects of Ionic Liquids*; Wiley-Interscience: New York, 2005.

(5) Dupont, J.; de Souza, R. F.; Suarez, P. A. Z. *Chem. Rev.* **2002**, *102*, 3667.
(6) Anderson, J. L.; Ding, J.; Welton, T.; Armstrong, D. W. *J. Am. Chem. Soc.* **2002**, *124*, 14247.
(7) Matsumoto, K.; Hagiwara, R. *J. Fluorine Chem.* **2007**, *128*, 317 and references therein.
(8) Armand, M.; Endres, F.; MacFarlane, D. R.; Ohno, H.; Scrosati, B. *Nature Mater.* **2009**, *8*, 621.
(9) Galiński, M.; Lawandowski, A.; Stępaniak, I. *Electrochim. Acta* **2006**, *51*, 5567.
(10) Ito, S.; Zakeeruddin, S. M.; Humphry-Baker, R.; Liska, P.; Charvet, R.; Comte, P.; Nazeeruddin, M. K.; Pechy, P.; Takata, M.; Miura, H.; Uchida, S.; Gratzel, M. *Adv. Mater.* **2006**, *18*, 1202.
(11) Ohno, H.; Ito, K. *Chem. Lett.* **1998**, 751.
(12) Ohno, H. *Bull. Chem. Soc. Jpn.* **2006**, *79*, 1665 and references therein.
(13) Kim, T. Y.; Lee, H. W.; Stoller, M.; Dreyer, D. R.; Bielawski, C. W.; Ruoff, R. S.; Suh, K. S. *ACS Nano* **2011**, *5*, 436.
(14) Marcilla, R.; Mecerreyes, D.; Winroth, G.; Brovelli, S.; Yebra, M. M. R.; Cacialli, F. *Appl. Phys. Lett.* **2010**, *96*, 043308.
(15) Huang, J.; Tao, C.; An, Q.; Zhang, W.; Wu, Y.; Li, X.; Shen, D.; Li, G. *Chem. Commun.* **2010**, *46*, 967.
(16) Lu, J.; Yan, F.; Texter, J. *Prog. Polym. Sci.* **2009**, *34*, 431.
(17) Green, O.; Grubjesic, S.; Lee, S.; Firestone, M. A. *Polym. Rev.* **2009**, *49*, 339.
(18) Green, M. D.; Long, T. E. *Polym. Rev.* **2009**, *49*, 291.
(19) Yuan, J.; Antonietti, M. *Polymer* **2011**, *52*, 1469.
(20) Mecerreyes, D. *Prog. Polym. Sci.* **2011**, DOI: 10.1016/j.progpolymsci.2011.05.007.
(21) Ye, Y.; Elabd, Y. A. *Polymer* **2011**, *52*, 1309.
(22) Chen, H.; Elabd, Y. A. *Macromolecules* **2009**, *42*, 3368.
(23) Chen, H.; Choi, J.; Salas-de la Cruz, D.; Winey, K. I.; Elabd, Y. A. *Macromolecules* **2009**, *42*, 4809.
(24) Marcilla, R.; Blazquez, A.; Rodriguez, J.; Pomposo, J. A.; Mecerreyes, D. *J. Polym. Sci., Part A* **2004**, *42*, 208.
(25) Marcilla, R.; Blazquez, J. A.; Fernandez, R.; Grande, H.; Pomposo, J. A.; Mecerreyes, D. *Macromol. Chem. Phys.* **2005**, *206*, 2999.
(26) Hara, M., Ed. *Polyelectrolytes: Science and Technologies*; Marcel Dekker: New York, 1992.
(27) Nakamura, K.; Saiwaki, T.; Fukao, K. *Macromolecules* **2010**, *43*, 6092.
(28) Ferry, J. D. *Viscoelastic Properties of Polymers*, 3rd ed.; John Wiley: New York, 1980.
(29) Doi, M.; Edwards, S. F. *The Theory of Polymer Dynamics*, 3rd ed.; Wiley: New York, 1980.
(30) Onogi, S.; Masuda, T.; Kitagawa, K. *Macromolecules* **1970**, *3*, 109.
(31) Horinaka, J.; Honda, S.; Takigawa, T. *Carbohydr. Polym.* **2009**, *78*, 576.
(32) Sammons, R. J.; Collier, J. R.; Rials, T. G.; Petrovan, S. *J. Appl. Polym. Sci.* **2008**, *110*, 1175.
(33) Gu, Y.; Lodge, T. P. *Macromolecules* **2011**, *44*, 1732.
(34) Eisenberg, A.; Kim, J.-S. *Introduction to Ionomers*; Wiley-Intersciene: New York, 1998.
(35) Brandrup, J.; Immergut, E. H.; Grulke, E. A. *Polymer HandBook*, 4th ed.; Wiley: New York, 1999.
(36) Hutcheson, S. A.; McKenna, G. B. *J. Chem. Phys.* **2008**, *129*, 074502.
(37) Schröter, K.; Hutcheson, S. A.; Shi, X.; Mandanici, A.; McKenna, G. B. *J. Chem. Phys.* **2006**, *125*, 214507.
(38) Iwawaki, H.; Nakamura, Y.; Inoue, T. *Macromolecules* **2011**, *44*, 5414.
(39) Williams, W. L.; Landel, R. F.; Ferry, J. D. *J. Am. Chem. Soc.* **1955**, *77*, 3701.
(40) Rubinstein, M.; Colby, R. H. *Polymer Physics*; Oxford University Press: London, 2003.
(41) Lee, M.; Choi, U. H.; Salas-de la Cruz, D.; Mittal, A.; Winey, K. I.; Colby, R. H.; Gibson, H. W. *Adv. Funct. Mater.* **2011**, *21*, 708.
(42) Nakamura, K.; Shikata, T. *ChemPhysChem* **2010**, *11*, 285.
(43) Li, C.; Register, R. A.; Cooper, S. L. *Polymer* **1989**, *30*, 1227.
(44) Eisenberg, A.; Hird, B.; Moore, R. B. *Macromolecules* **1990**, *23*, 4098.
(45) Longworth, R.; Vaughan, D. J. *Nature* **1968**, *218*, 85.
(46) Jiang, M.; Gronowski, A. A.; Yeager, H. L.; Wu, G.; Kim, J.-S.; Eisenberg, A. *Macromolecules* **1994**, *27*, 6541.
(47) Tudryn, G. J.; Liu, W.; Wang, S.-W.; Colby, R. H. *Macromolecules* **2011**, *44*, 3572.
(48) Eisenberg, A.; Navratil, M. *Macromolecules* **1973**, *6*, 604.
(49) Kim, J.-S.; Jackman, R. J.; Eisenberg, A. *Macromolecules* **1994**, *27*, 2789.
(50) Vanhoorne, P.; Register, R. A. *Macromolecules* **1996**, *29*, 598.
(51) Weiss, R. A.; Fitzgerald, J. J.; Kim, D. *Macromolecules* **1991**, *24*, 1071.
(52) Leibler, L.; Rubinstein, M.; Colby, R. H. *Macromolecules* **1991**, *24*, 4701.
(53) Colby, R. H.; Zheng, X.; Rafailovich, M. H.; Sokolov, J.; Peiffer, D. G.; Schwarz, S. A.; Strzhemechny, Y.; Nguyen, D. *Phys. Rev. Lett.* **1998**, *81*, 3876.
(54) Weiss, R. A.; Zhao, H. *J. Rheol.* **2009**, *53*, 191.
(55) Masuda, T.; Kitagawa, K.; Inoue, T.; Onogi, S. *Macromolecules* **1970**, *3*, 116.
(56) Wübbenhorst, M.; van Turnhout, J. *J. Non-Cryst. Solids* **2002**, *305*, 40.
(57) Strobl, G. R. *The Physics of Polymers: Concepts for Understanding Their Structures and Behavior*, 3rd ed.; Springer: New York, 2007.
(58) Roland, C. M.; Ngai, K. L.; Plazek, D. J. *Macromolecules* **2004**, *37*, 7051.
(59) Fragiadakis, D.; Dou, S.; Colby, R. H.; Runt, J. *Macromolecules* **2008**, *41*, 5723.